Semenogelin-1 Inhibition of Mouse Sperm Hyperactivation Reveals Two Functional Domains Modulating CatSper Channel

Noemia A. P. Mariani[1], Natália C. M. Santos[1], Juliana J. Andrade[1], Alexandre D. Andrade[1], Beatriz Rezende[1], Tomás J. Steeman[2], Analia G. Novero[2], José C. de Lima-Junior[3], Giulia Calderaro[1], Ana Clara F. Themer[1], Hélio Kushima[1], Mariano G. Buffone[5], Darío Krapf[2], Polina V. Lishko[3,4], Erick J. R. Silva[1]*.

[1]Department of Biophysics and Pharmacology, Biosciences Institute of Botucatu, São Paulo State University, Botucatu, SP, Brazil; [2]Institute of Molecular and Cellular Biology of Rosario, Rosario, SF, Argentina; [3]Department of Cell Biology and Physiology, Washington University in St. Louis, School of Medicine, St. Louis, MO, United States; [4]Center for the Investigation of Membrane Excitability Diseases (CIMED), WashU Medicine, St. Louis, MO, United States; [5]Institute of Biology and Experimental Medicine, Buenos Aires, BA, Argentina.

* Corresponding author: E-mail: ejr.silva@unesp.br.

Running title: SEMG1 inhibition of sperm hyperactivation.

Keywords: Sperm motility; Epididymal protease inhibitor; Spermatozoon; Ion Channels; Seminal Plasma; Semenogelins.

Abstract

Seminal plasma is essential for sperm survival and function after ejaculation. Semenogelin-1 (SEMG1), the predominant seminal plasma protein, transiently suppresses sperm motility and hyperactivation after ejaculation through epididymal protease inhibitor (EPPIN) binding. However, the molecular mechanism underlying SEMG1-mediated inhibition of hyperactivation remains unclear. Here, we tested the hypothesis that SEMG1 inhibits CatSper, a sperm-specific calcium channel crucial for hyperactivation. Full-length recombinant mouse SEMG1 (mSEMG1; Q32-G375) inhibited both progressive motility and hyperactivation; the latter was not recovered with NH_4Cl-induced alkalinization, indicating an effect downstream of capacitation-associated intracellular alkalinization. Electrophysiological recordings revealed that mSEMG1 reduced CatSper currents at physiologically relevant concentrations. Truncated mSEMG1 fragments mSEMG1$^{Q32\text{-}V118}$ and mSEMG1$^{R98\text{-}G375}$, but not mSEMG1$^{Y221\text{-}G375}$, inhibited sperm hyperactivation and CatSper currents to a similar extent as full-length mSEMG1. Notably, only mSEMG1$^{R98\text{-}G375}$ retained full EPPIN-binding capacity. Together, our findings identify two functional domains within mSEMG1 (Q32-V118 and R98-S220) that inhibit sperm hyperactivation by suppressing CatSper activity and differ in their EPPIN-binding capacities. These functional domains represent promising prototypes for the design of spermiostatic molecules, offering additional avenues for non-hormonal male contraception.

Summary statement

We report a novel mechanism by which SEMG1, a major seminal plasma protein, modulates sperm hyperactivation by inhibiting a key calcium channel, offering new insights into sperm function and non-hormonal male contraception.

Introduction

To successfully fertilize the egg, spermatozoa must undergo their final maturation within the female reproductive tract, in a process named capacitation (Chang, 1951; Austin, 1952; Stival et al., 2016; Freitas et al., 2017). Sperm capacitation entails a complex cascade of molecular events, including cholesterol efflux from the plasma membrane, tyrosine phosphorylation of sperm proteins, increases in intracellular pH (pH_i) and Ca^{2+} concentrations ($[Ca^{2+}]_i$), as well as membrane hyperpolarization. Sperm capacitation allows spermatozoa to undergo acrosome exocytosis in response to appropriate stimuli and to transition from progressive motility to a vigorous, asymmetric, whip-like flagellar motion known as hyperactivation (López-González et al., 2014; Freitas et al., 2017; Ritagliati et al., 2018; Vyklicka and Lishko, 2020).

Among the molecular pathways involved in sperm hyperactivation, the rise in intracellular Ca^{2+} levels is critical (Darszon et al., 2011). Even though multiple mechanisms promote Ca^{2+} influx in spermatozoa, the activation of the voltage-dependent and alkalinization-activated Ca^{2+} channel CatSper is considered the most relevant (Lishko and Mannowetz, 2018). The CatSper channel consists of a complex of at least fourteen proteins: four pore-forming subunits (CatSper1–4) and 10 accessory subunits (CatSper β, γ, δ, ε, ζ τ, η, θ, EFCAB9, and transporter SLCO6C1) (Lishko and Mannowetz, 2018; Hwang et al., 2019; Lin et al., 2021). This large multiprotein complex, known as CatSpermasome, is arranged as four longitudinal lines spanning the entire length of the sperm principal piece, facilitating structural and functional coupling between CatSper complexes and triggering powerful Ca^{2+} waves along the sperm flagellum (Bystroff, 2018; Vyklicka and Lishko, 2020; Lin et al., 2021; Zhao et al., 2022). Notably, CatSper deficiency in men and rodents leads to infertility due to a failure of sperm hyperactivation, while no other phenotypical abnormalities are observed (Carlson et al., 2005; Avenarius et al., 2009; Hildebrand et al., 2010; Chung et al., 2017).

While sperm hyperactivation is crucial for fertilization, it must remain tightly regulated until spermatozoa reach the oviduct (De Jonge, 2017). In this context, seminal plasma components play critical roles in modulating sperm hyperactivation and other capacitation-associated events (Vickram et al., 2022). Semenogelin-1 (SEMG1), the predominant protein in seminal plasma, is secreted by the seminal vesicles and incorporated onto the sperm surface during ejaculation through its interaction with epididymal protease inhibitor (EPPIN) in both humans and rodents (Wang et al., 2005; Silva et al., 2012; Silva et al., 2013; Mariani et al., 2020). SEMG1 binds to freshly ejaculated spermatozoa, acting as a decapacitation factor and blocking sperm motility, hyperactivation, and acrosome exocytosis (Kawano and Yoshida, 2007; de Lamirande and Lamothe, 2010; Mitra et al., 2010; Araki et al., 2015). In humans, this inhibitory effect is maintained until the serine protease prostate-specific antigen (PSA) cleaves SEMG1, resulting in semen liquefaction and activation of sperm motility (Robert and Gagnon, 1999). Furthermore, SEMG1 promotes sperm survival in the uterus, as evidenced by the low viability of

79 spermatozoa from *Semg1*$^{-/-}$ mice collected from the female reproductive tract during natural mating,
80 causing a severe subfertility phenotype (Kawano et al., 2014). Together, these findings indicate that
81 SEMG1 has a dual role of protecting and modulating sperm function and metabolism during their journey
82 through the female reproductive tract. However, the precise molecular mechanisms underlying
83 SEMG1's roles and the contribution of EPPIN binding to these effects remain poorly understood.
84 Initial studies have shown inhibitory effects of SEMG1 on sperm pH_i and $[Ca^{2+}]_i$ (O'Rand and
85 Widgren, 2012). Building upon these findings, we hypothesize that SEMG1 inhibits CatSper activity,
86 thereby altering Ca^{2+} homeostasis and downstream pathways required for sperm hyperactivation. To
87 test this hypothesis, we investigated the effects of recombinant mouse SEMG1 (mSEMG1) on sperm
88 motility, hyperactivation, and CatSper currents. We further investigated the contribution of distinct
89 SEMG1 domains and assessed the relevance of EPPIN binding in mediating their effects. Our results
90 revealed that mSEMG1 inhibits hyperactivation by modulating CatSper currents, an effect mediated by
91 distinct domains within the Q32-V118 and R98-S220 sequences. Remarkably, only the R98-S220
92 sequence bound EPPIN to the full extent, indicating that SEMG1 regulates sperm hyperactivation
93 through domain-specific mechanisms associated with differential EPPIN interaction. Our findings
94 provide novel mechanistic insights into how mSEMG1 prevents premature sperm hyperactivation and
95 open avenues for exploring its functional domains as templates for the rational design of ligands with
96 male contraceptive applications targeting spermatozoa.
97
98 **Results**
99 **Mouse SEMG1 inhibits sperm progressive and hyperactivated motilities**
100 The sperm motility pattern changes from progressive to hyperactivated upon capacitation (Katz and
101 Yanagimachi, 1980; Suárez and Osman, 1987). Previous studies have shown that both human and
102 mouse SEMG1 can regulate sperm function, including motility (Mitra et al., 2010; Silva et al., 2013;
103 Sakaguchi et al., 2020). To gain insights into the effects of SEMG1 on sperm swimming behavior, we
104 incubated murine spermatozoa isolated from the cauda epididymidis in capacitating medium, in either
105 the absence (control) or in the presence of increasing concentrations of full-length recombinant mouse
106 SEMG1 (mSEMG1; Q32-G375). mSEMG1 reduced sperm motility only at 25 μM (~25% inhibition) after
107 20 min ($p = 0.0005$) and 120 min ($p = 0.011$) of incubation compared to the control (Fig. 1A, Fig. S1,
108 Video S1). Concurrently, mSEMG1 increased the percentage of slow-motile spermatozoa at 10 μM (p
109 $= 0.026$) and 25 μM ($p = 0.001$) after 20 min of incubation compared to the control (Fig. 1B, Fig. S1).
110 mSEMG1 did not affect sperm viability at the concentrations tested, confirming that its effects on sperm
111 motility were not associated with sperm death (Fig. 1C).
112 mSEMG1 displayed a more potent inhibitory effect on hyperactivated motility by inducing a
113 concentration-dependent inhibition with an IC_{50} of 5.2 μM (95% confidence interval; 95% CI 1.3–21.2

114 μM). The maximum inhibition of ~90% was reached at 25 μM ($p = 0.0003$) after 120 min, compared to
115 the control (Fig. 2A, B). Consistently, 25 μM mSEMG1 decreased curvilinear velocity (VCL, $p = 0.006$)
116 and amplitude of lateral head displacement (ALH, $p = 0.005$), kinematic parameters associated with
117 vigorous sperm movements (Cancel et al., 2000) (Fig. 2C). Notably, mSEMG1 effects on hyperactivation
118 were not rescued by intracellular alkalization induced by NH_4Cl (Fig. 2D), a condition that enhance
119 sperm hyperactivation via alkalinization evoked activation of CatSper (Ren et al., 2001; Kirichok et al.,
120 2006) (Fig. 2D). Similarly, mSEMG1 inhibited progressive motility (IC_{50} 10.1 μM, 95% CI 2.6–38.5 μM),
121 and decreased both average path velocity (VAP) and straight-line velocity (VSL), kinematic parameters
122 associated with sperm progressiveness (Fig. S2). Altogether, these results indicate that mSEMG1
123 inhibits mouse sperm progressive motility and hyperactivation by modulating signaling pathways
124 downstream of intracellular alkalinization.
125
126 **Mouse SEMG1 is a CatSper channel inhibitor**
127 Activation of CatSper channel leads to a rise in intracellular Ca^{2+} concentration, which is essential
128 for the development of hyperactivated motility in both murine and human spermatozoa (Quill et al., 2003;
129 Carlson et al., 2005; Young et al., 2024). Thus, we decided to explore whether mSEMG1 inhibits
130 hyperactivation by affecting the CatSper channel. To do so, we conducted whole-cell patch clamp
131 experiments using non-capacitated murine spermatozoa to record CatSper currents ($I_{CatSper}$) in the
132 absence or presence of mSEMG1.
133 $I_{CatSper}$ were elicited by voltage ramps from -80 to +80 mV from a holding potential of 0 mV (Fig. 3A).
134 Under these conditions, no CatSper current was detected in a high-saline (HS) extracellular bath
135 solution containing Ca^{2+} and Mg^{2+} (Table S1), which represents the baseline recording (Fig. 3B). The
136 remaining current under this condition was attributed to a leak current and was negligible. Upon
137 perfusion with divalent-free Cs^{+}-based (DVF) bath solution (Table S2), the characteristic monovalent
138 CatSper current was recorded, as previously described (Kirichok and Lishko, 2011; Liu et al., 2021)
139 (Fig. 3B) . Following the DVF perfusion, sperm cells were exposed to 5 μM mSEMG1, which suppressed
140 both inward and outward CatSper currents (Fig. 3B, C). After subtracting the leak currents, the averaged
141 (± standard error of the mean, s.e.m.) control inward $I_{CatSper}$ in DVF at -80 mV was 218.4 ± 31.7 pA (Fig.
142 3B). Under the same conditions, exposure to 5 μM mSEMG1 inhibited the inward $I_{CatSper}$ to 150.8 ± 23.4
143 pA (~31% suppression; $p = 0.019$) (Fig. 3B). No currents were detected when spermatozoa from
144 *CatSper1*$^{-/-}$ mice were tested either in the absence or presence of mSEMG1 (Fig. 3B, insert). mSEMG1
145 inhibition was reversible as CatSper conductance recovered upon continuous washing in DVF (177.0 ±
146 17.2 pA; $p = 0.378$) (Fig. 3B).
147 In addition to intracellular alkalization, CatSper is sensitive to membrane voltage (Kirichok et al.,
148 2006; Vyklicka and Lishko, 2020). During capacitation, the sperm plasma membrane undergoes

149 hyperpolarization via the sperm-specific and pH-sensitive K^+ channel SLO3, which in turn is activated
150 by alkaline intracellular pH (Mannowetz et al., 2013). Therefore, we tested the effect of reduced $I_{CatSper}$
151 caused by mSEMG1 on membrane potential (Em) during sperm capacitation. As expected, capacitated
152 spermatozoa displayed a more negative membrane potential in comparison to non-capacitated
153 spermatozoa (Fig. 3D, Fig. S3). Capacitation-induced membrane hyperpolarization was not affected in
154 the presence of 10 μM mSEMG1 (Fig. 3D, Fig. S3). These results indicate that mSEMG1 inhibits
155 CatSper activity at low micromolar concentrations comparable to those required to inhibit sperm
156 hyperactivation, without affecting the Em.
157

158 **Mouse SEMG1 Q32-V118 and R98-S220 sequences independently contribute to the inhibition of**
159 **sperm hyperactivation and CatSper currents**

160 Despite the low conservation in their primary sequences, both human and mouse SEMG1 exhibit a
161 single cysteine residue (C239 in human SEMG1 and C97 in mouse SEMG1), as well as internal
162 repetitive amino acid sequences. Downstream of the cysteine residue, mouse SEMG1 contains two 31-
163 amino acid repeats (K119-S149 and K177-S207) and multiple short repeats of two (KS), three (GGS),
164 or six-eight (QVKSSVSQ or QVKSSGSQ) amino acid residues that become less frequent toward its C-
165 terminal region (Fig. 4A). Previous studies demonstrated that sequences within human SEMG1 that are
166 part of long repeats and flank the cysteine residue are essential for its interaction with spermatozoa,
167 EPPIN binding, and modulation of sperm motility (Mitra et al., 2010; Silva et al., 2013). Based on these
168 observations, we obtained three truncated mSEMG1 constructs (i) $mSEMG1^{Q32\text{-}V118}$, which contains its
169 unique cysteine residue, (ii) $mSEMG1^{R98\text{-}G375}$, which lacks the cysteine residue but includes the two long
170 repeats, and (iii) $mSEMG1^{Y221\text{-}G375}$, which lacks both the cysteine residue and the long repeats (Fig. 4A),
171 allowing us to evaluate the relevance of these sequences to the inhibition of sperm hyperactivation.

172 Neither of the truncated mSEMG1 constructs affected sperm motility in a significant manner (Fig.
173 4B). Nevertheless, $mSEMG1^{Q32\text{-}V118}$ and $mSEMG1^{R98\text{-}G375}$, but not $mSEMG1^{Y221\text{-}G375}$, inhibited
174 hyperactivated motility compared to the control ($p = 0.004$ and 0.028, respectively) to a similar extent
175 as the full-length mSEMG1 (Fig. 4B, C, Fig. S4, Video S2). $mSEMG1^{Q32\text{-}V118}$ also reduced the associated
176 kinematic parameter VCL ($p = 0.029$), and a similar trend was observed for $mSEMG1^{R98\text{-}G375}$ ($p = 0.084$)
177 (Fig. 4C). Consistent with these findings, both $mSEMG1^{Q32\text{-}V118}$ and $mSEMG1^{R98\text{-}G375}$ suppressed inward
178 and outward $I_{CatSper}$ (Fig. 5A, B, Fig. S5). $mSEMG1^{Y221\text{-}G375}$ also inhibited CatSper, albeit to a lesser extent
179 than the rest of the truncated constructs (Fig. 5A-C, Fig. S5). At 5 μM concentration, $mSEMG1^{Q32\text{-}V118}$,
180 $mSEMG1^{R98\text{-}G375}$, and $mSEMG1^{Y221\text{-}G375}$ suppressed the inward $I_{CatSper}$ at -80 mV to values equivalent to
181 ~56%, ~66%, and ~77% of those observed with their respective controls, corresponding to mean
182 differences of of 93.6 ($p = 0.007$), 108.6 ($p < 0.0001$), and 55.9 pA ($p = 0.011$), respectively (Fig. 5A-C,
183 Fig. S5). These results indicate that sequences within the mSEMG1 Q32-V118 and R98-S220 regions,

184 which encompass cysteine and the long repeats, contain domains sufficient to inhibit sperm
185 hyperactivation through CatSper inhibition.
186
187 **Mouse SEMG1 R98-G220 sequence contains the main EPPIN binding domain**
188 Our previous study demonstrated the co-immunoprecipitation and co-localization of SEMG1 and
189 EPPIN in mouse spermatozoa pre-incubated with seminal vesicle fluid, suggesting that EPPIN serves
190 as a docking site for SEMG1 on the mouse sperm surface (Mariani et al., 2020). Here, we confirmed
191 the interaction between mouse EPPIN and SEMG1 using the AlphaScreen (Amplified Luminescent
192 Proximity Homogeneous Assay Screen) assay (Fig. 6A), which has been previously employed to
193 investigate the binding of human EPPIN and SEMG1 (Silva et al., 2012; Silva et al., 2013). Using
194 mSEMG1 and full-length recombinant mouse EPPIN (mEPPIN; L24-T134), we observed a maximum
195 interaction signal peaking at 2 h and remaining stable for at least 8 h (Fig. 6B). The interaction signals
196 showed a concentration-dependent pattern when mSEMG1 and mEPPIN were titrated, with calculated
197 EC_{50} (95% CI) of 23.6 nM (20.0–27.8 nM) and 1.0 nM (0.3–3.3 nM), respectively (Fig. 6C). Interestingly,
198 when recombinant human SEMG1 (hSEMG1, G26-R281) replaced mSEMG1, we observed a
199 concentration-dependent saturable binding curve, with a calculated EC_{50} of 8.3 nM (6.8–18.5 nM),
200 confirming the conservation of the EPPIN binding sites in human and mouse SEMG1 sequences (Fig.
201 S6).
202 To map the EPPIN binding site, we tested the mEPPIN binding capacity of our truncated mSEMG1
203 constructs. $mSEMG1^{R98-G375}$ showed a mEPPIN binding capacity similar to the full-length mSEMG1,
204 both displaying a comparable specific signal (Fig. 6D). In contrast, we observed a reduction in the
205 specific signal by ~80% ($p < 0.0001$) and ~69% ($p < 0.0001$) for $mSEMG1^{Q32-V118}$ and $mSEMG1^{Y221-G375}$
206 in comparison to full-length mSEMG1, respectively (Fig. 6D).
207 In addition, the removal of mouse EPPIN Kunitz domain in a C-terminal truncation lacking residues
208 C69-T134 resulted in a reduction in the specific signal by ~75% ($p = 0.001$) compared to that detected
209 with full-length EPPIN (Fig. 6D). Competition assays using anti-EPPIN antibodies Q20E and S21C, that
210 recognized epitopes within EPPIN WFDC and Kunitz domains, respectively, reduced the specific signal
211 of the binding of mEPPIN and mSEMG1 in a concentration-dependent manner with IC_{50} values of 3.0
212 nM (0.2–34.3 nM) and 95.6 nM (20.6–443.6 nM), respectively (Fig. S7). Altogether, these results
213 demonstrate that the sequence R98-S220 of mSEMG1 contains the major mEPPIN binding domain and
214 that both WFDC and Kunitz domains of mEPPIN are involved in mSEMG1 binding.
215
216 **Discussion**
217 During ejaculation, SEMG1 coats the sperm surface by interacting with EPPIN, thereby modulating
218 sperm motility and preventing capacitation-associated events, such as hyperactivation and acrosome

219 exocytosis (O'Rand et al., 2011; Vickram et al., 2022). However, the underlying mechanisms governing
220 the effects of SEMG1 on sperm function remain elusive. Here, we demonstrate that mSEMG1 inhibited
221 sperm hyperactivation at concentrations at least 200-fold lower than those previously reported
222 (Sakaguchi et al., 2020), highlighting SEMG1 as a potent, endogenous inhibitor of sperm
223 hyperactivation. Moreover, our results reveal that mouse SEMG1 contains two distinct functional
224 domains – within the Q32-V118 and R98-S220 sequences – which inhibit sperm hyperactivation by
225 targeting CatSper. Since only the R98-S220 sequence retained full-extent EPPIN binding capacity
226 relative to full-length mSEMG1, our data indicate that SEMG1 operates through domain-specific
227 mechanisms associated with differential EPPIN interaction.

228 During capacitation, murine spermatozoa experience a pH_i shift from acidic to alkaline, primarily
229 driven by Na^+/H^+ exchangers (NHEs) (Wang et al., 2007; Novero et al., 2024). This event is crucial for
230 the activation of sperm-specific ion channels, such as CatSper, which in turn leads to a rise in $[Ca^{2+}]_i$
231 (Lishko and Mannowetz, 2018; Ritagliati et al., 2018). Ca^{2+} influx through CatSper plays a fundamental
232 role in reproduction, as the channel dysfunction leads to male infertility associated with hyperactivation
233 failure in both humans and mice (Wang et al., 2021). While previous reports have demonstrated that the
234 inhibition of sperm motility by SEMG1 was related to a decrease in $[Ca^{2+}]_i$ (O'Rand and Widgren, 2012),
235 the direct association of CatSper in this process has not been clarified. As shown herein, mSEMG1
236 exerts inhibitory effects on hyperactivation through inhibition of CatSper currents, thereby revealing a
237 novel regulatory mechanism for CatSper activity promoted by a seminal plasma protein.

238 Given that intracellular alkalization is a well-established trigger for CatSper activation and sperm
239 hyperactivation (Kirichok et al., 2006), we investigated whether pharmacologically induced pH_i increase
240 could rescue hyperactivation following mSEMG1 treatment. Our findings showed that hyperactivated
241 motility remained suppressed despite pH_i alkalization, indicating a downstream effect of alkalinization-
242 dependent CatSper activation. During capacitation, increases in $[Ca^{2+}]_i$ contribute to both Em
243 hyperpolarization and intracellular alkalinization, forming a positive feedback loop that in turn potentiates
244 CatSper activity (Chávez et al., 2014; Novero et al., 2024). In this regard, Em hyperpolarization is
245 mediated by KSper, which localizes along the sperm flagellum (Navarro et al., 2007; Mannowetz et al.,
246 2013). mSEMG1 did not alter Em hyperpolarization during sperm capacitation, indicating that it does
247 not affect KSper activity. Given the relevance of Em hyperpolarization for acrosome exocytosis, our
248 results highlight the relevance of further investigating the role of SEMG1 on this crucial sperm event in
249 future studies.

250 In the normal physiological context, mouse SEMG1 is present in the seminal plasma at higher
251 concentrations (≥ 25 μM; Kawano and Yoshida, 2007) than those required for inhibiting sperm
252 hyperactivation *in vitro*. Thus, our findings support the model that SEMG1 can effectively prevent
253 premature hyperactivation by limiting CatSper activity in ejaculate spermatozoa, through mechanisms

254 that do not rely on upstream changes in pH_i or Em. Whether SEMG1 inhibits CatSper through direct
255 interaction with channel subunits or indirectly via protein–protein interactions, or inhibition of specific
256 signaling pathways remains to be determined. One putative mechanism involves the ability of SEMG1
257 to stabilize membrane microdomains through modulation of cholesterol removal and binding to lipid raft
258 components, such as the ganglioside GM1 (Kawano et al., 2008), which may in turn affect capacitation-
259 associated membrane modifications and modulate CatSper activity. Further experimental evidence is
260 required to test this hypothesis.

261 Our findings identified two functional domains within the mSEMG1, spanning Q32-V118 and R98-
262 S220 sequences, that play crucial roles in inhibiting sperm hyperactivation. Truncated constructs
263 containing these sequences promoted inhibition of CatSper activity to a similar extent as the full-length
264 mSEMG1. These findings are consistent with previous observations that SEMG1 is a modular protein,
265 containing discrete domains that contribute to its multifunctional roles in sperm function and protection
266 (de Lamirande, 2007; Vickram et al., 2022). Upon ejaculation, SEMG1 associates with the sperm
267 surface through binding to EPPIN, a process known to be critical for regulating sperm motility (Mitra et
268 al., 2010; O'Rand et al., 2011; O'Rand and Widgren, 2012). Our previous results demonstrated the co-
269 immunoprecipitation of EPPIN and SEMG1 from mouse spermatozoa incubated with the seminal vesicle
270 fluid when either anti-EPPIN or anti-SEMG1 antibodies were used, indicating a parallel system to
271 humans (Wang et al., 2005; Mariani et al., 2020). These observations prompted us to investigate the
272 relevance of EPPIN binding to the effects of mSEMG1 on sperm function. Our data showed that mouse
273 EPPIN and SEMG1 are binding partners, confirming that EPPIN is a docking site for SEMG1 on the
274 mouse sperm surface, and further demonstrated functional conservation of this interaction by
275 demonstrating that mouse EPPIN can also bind human SEMG1.

276 We identified the mSEMG1 R98-S220 sequence, which lacks its unique cysteine residue but
277 encompasses two long amino acid repeats, as containing the major EPPIN binding domain. This result
278 was unexpected, since human SEMG1 relies on amino acid sequences flanking its unique cysteine
279 residue to bind EPPIN and inhibit sperm motility (Silva et al., 2013). This divergence may reflect the
280 rapid adaptive evolution of *SEMG1* genes across species (Ferreira et al., 2013; Silva et al., 2013), which
281 could shift EPPIN-binding pockets to different regions of the primary sequence when mouse and human
282 SEMG1 are compared. Conversely, the mSEMG1 Q32–V118 sequence, which contains its unique
283 cysteine residue, displayed low EPPIN binding *in vitro* (<20% relative to the full-length mSEMG1), yet
284 retained the ability to inhibit CatSper currents and sperm hyperactivation. These findings indicate that
285 different mSEMG1 domains inhibit sperm hyperactivation and that strong EPPIN binding is not strictly
286 required for CatSper inhibition by this SEMG1 fragment once present at the sperm surface.
287 Nevertheless, we cannot rule out the possibility that EPPIN binding may facilitate the initial positioning
288 of both mSEMG1 R98-S220 and Q32–V118 sequences on the sperm surface, enabling distinct SEMG1

289 domains to engage downstream targets, such as CatSper. Importantly, recent genetic studies show that
290 the combined ablation of *Eppin* and its paralogs *Wfdc6a*, *Wfdc8*, and *Wfcd6b* in mice led to an
291 azoospermic phenotype, underscoring the essential role of EPPIN in sperm development but precluding
292 a direct functional testing of mSEMG1 effects in mature spermatozoa lacking EPPIN (Kent et al., 2024).
293 Altogether, we conclude that mouse SEMG1 may inhibit CatSper and hyperactivation through domain-
294 specific mechanisms associated with differential EPPIN-binding capacity.
295 Based on our findings, we propose a working model by which SEMG1 regulates hyperactivation in
296 ejaculated spermatozoa in mice (Fig. 7). Following ejaculation, SEMG1 coats the surface of
297 spermatozoa through EPPIN binding in the semen coagulum/copulatory plug, preventing premature
298 hyperactivation and capacitation within the female reproductive tract. This event is mediated by two
299 distinct SEMG1 functional domains within Q32-V118 and R98-S220 sequences that inhibit CatSper
300 activity through domain-specific mechanisms. In the oviduct, a putative PSA-like protease (likely
301 belonging to the kallikrein family) cleaves SEMG1, allowing spermatozoa to undergo hyperactivation
302 and capacitation. Collectively, these findings position SEMG1 Q32-V118 and R98-S220 sequences as
303 compelling prototypes for the rational design of CatSper inhibitors with potential applications in male
304 contraception targeting critical regulatory pathways for hyperactivation.
305
306 **Experimental Procedures**
307 **Animals**
308 We used male (90–120 days old) and female (60–90 days old) Swiss mice obtained from the Center
309 for Research and Production of Laboratory Animals (CPPA) of São Paulo State University, Botucatu,
310 SP, Brazil. The animals were maintained under controlled conditions (12 h light/dark cycle, 22–24°C)
311 with food and water available ad libitum. All procedures were approved by the Animal Care and Use
312 Committee of UNESP (protocol #5219150420) and followed the guidelines of the Brazilian National
313 Council for the Control of Animal Experimentation (CONCEA). We also used wild-type (WT) and
314 CatSper1-deficient male C57BL/6 mice, maintained at the Animal Facility of Washington University in
315 St. Louis, School of Medicine, St. Louis, MO, United States (protocol #22-0251), and the Facultad de
316 Ciencias Bioquímicas y Farmacéuticas de Rosario, Rosario, SF, Argentina (protocol #492/2018). These
317 animals were used for patch-clamp recordings, membrane potential analysis, and additional sperm
318 motility experiments. All experiments were conducted following the institutional guidelines for animal
319 research and were approved by the respective Animal Care and Use Committees. Mice were euthanized
320 by inhaled isoflurane overdose or CO_2 inhalation, followed by cervical dislocation.
321
322 **Protein-protein interaction assays**

323 We performed AlphaScreen to evaluate protein–protein interactions as previously described (Silva
324 et al., 2012), with the following modifications. Briefly, recombinant mEPPIN and its N-terminal fragment,
325 both containing an N-terminal GST-tag, were pre-incubated with anti-GST acceptor beads for 60
326 minutes. In parallel, mSEMG1 and its truncated fragments (Fig. 4A), containing a 6x-His tag, were
327 incubated with Ni-NTA-chelate donor beads under the same conditions. Equal volumes of the
328 mEPPIN/acceptor bead suspension and the mSEMG1/donor bead suspension were transferred to white
329 opaque 384-well microplates (OptiPlate-384; PerkinElmer, Waltham, MA), in a final reaction volume of
330 30 µL per well. Plates were sealed and placed in a Synergy 2 Multiplatform automated plate reader
331 (BioTek, Winooski, VT). After 2 min of shaking, readings were taken every 2 h over 8 h, using a 680/30
332 excitation filter and a 570/100 emission filter. Data acquisition was performed using Gen5 software
333 (BioTek), and a total of 9 time points were recorded per experiment. All conditions were assayed in
334 triplicate.
335 Final concentrations of the assay components ranged from 0.1–10 nM for mEPPIN, 0.3–100 nM for
336 mSEMG1, and 10 µg/mL for the donor and acceptor beads. Negative controls were conducted under
337 the same conditions in the absence of either mEPPIN or mSEMG1, with beads only. The specific signal
338 at each time point was calculated by subtracting the background signal (obtained in the absence of one
339 of the proteins) from the total signal. To determine the EC_{50} for mEPPIN binding to mSEMG1, we applied
340 nonlinear regression curve fitting to the specific signal values obtained after 4 h of incubation. For
341 competition assays, we incubated mEPPIN (10 nM) and mSEMG1 (30 nM) in the presence of increasing
342 concentrations of anti-EPPIN Q20E (targeting the P20–E39 epitope) or anti-EPPIN S21C (targeting the
343 S103–C121 epitope) antibodies, maintaining a total reaction volume of 30 µL and bead concentration at
344 10 µg/mL. Specific signals for each competitor concentration were calculated as described, and IC_{50}
345 values were determined by nonlinear regression. The expression and purity of mEPPIN and mSEMG1
346 were confirmed by Western blot before the experiments (Fig. S4).
347
348 **Analysis of Sperm Motility**
349 Analysis of sperm motility was performed as previously described (Silva et al., 2021), with the
350 following modifications. We collected mouse spermatozoa from the cauda epididymides and incubated
351 them in human tubal fluid (HTF) medium at 37 °C under 5% CO_2. After 10 min of incubation, we removed
352 the tissue and diluted the sperm suspension (~40,000 cells) in HTF supplemented with 25 mM sodium
353 bicarbonate and 0.75% (m/v) bovine serum albumin (BSA; Sigma, cat. #SLBT1197). We treated the
354 sperm suspensions with recombinant mSEMG1 or its truncated constructs (1–25 µM) (Fig. 4). Negative
355 controls were prepared using HTF medium without recombinant proteins. Rescue experiments were
356 performed to assess whether intracellular alkalinization could counteract the inhibitory effects of
357 mSEMG1 on sperm motility. Alkalinization was induced by NH_4Cl addition, and its efficacy was verified

358 by analyzing sperm motility under non-capacitating conditions (medium lacking bicarbonate and BSA)
359 following NH_4Cl treatment. Sperm motility was analyzed using a computer-assisted sperm analysis
360 (CASA) system (Hamilton-Thorne, Beverly, MA, USA) with Animal Motility II Software version 1.9. We
361 acquired images using an Olympus CX41 microscope equipped with a MiniTherm stage warmer and a
362 JAI CM-040 digital camera. Aliquots of the sperm suspensions were loaded into pre-warmed 80-μm 2X-
363 CEL slides (Hamilton-Thorne) at 37°C using large-bore pipette tips. We assessed sperm motility at 20-
364 120 min after incubation.
365 We recorded sperm tracks for 1.5 s (90 frames) at a frame rate of 60 Hz using a 40× negative-phase
366 contrast objective. For each sample, we analyzed at least 200 spermatozoa across 10 different fields.
367 We used video playback to review and manually correct the tracks, removing mistracked cells caused
368 by collisions or debris interference. We then extracted individual ASCII files containing the kinematic
369 parameters for each sperm cell. The following parameters were analyzed: average path velocity (VAP,
370 mm/s), straight-line velocity (VSL, mm/s), curvilinear velocity (VCL, mm/s), amplitude of lateral head
371 displacement (ALH, μm), straightness (STR, %), and linearity (LIN, %). We classified sperm as
372 progressive when VAP > 50 μm s^{-1} and STR > 50%, hyperactivated when VCL > 180 50 μm s^{-1}, ALH
373 > 9.5 μm, and LIN < 23.6%, and slow when VAP ≤ 30 50 μm s^{-1} and VSL ≤ 50 μm s^{-1} (Silva et al., 2021).
374 To assess the potential effects of mSEMG1 and its fragments on sperm viability after the maximum
375 incubation period of 120 min under capacitating conditions, viability was evaluated in parallel with motility
376 assays using eosin-nigrosin staining.
377
378 **Electrophysiology**
379 Electrophysiological recordings were performed as previously described (Liu et al., 2021). In
380 summary, gigaohm seals were established at the cytoplasmic droplet of mouse sperm (Fig. 3) using HS
381 containing (in mM): 130 NaCl, 5 KCl, 1 $MgSO_4$, 2 $CaCl_2$, 5 glucose, 1 sodium pyruvate, 10 lactic acid,
382 and 20 HEPES (pH 7.4). Whole-cell configuration was achieved by applying brief (1 ms) voltage pulses
383 of 400–630 mV combined with gentle suction. Currents were elicited with voltage ramps from −80 mV
384 to +80 mV, starting from a holding potential of 0 mV, in both HS and divalent-free (DVF) bath solutions.
385 Data were acquired at a sampling rate of 2–5 kHz using a low-pass filter at 1 kHz. Patch pipettes (11–
386 17 MΩ) were filled with an internal solution containing (in mM): 130 Cs-methanesulfonate, 70 HEPES,
387 3 EGTA, 2 EDTA, and 0.5 Tris-HCl (pH adjusted to 7.4 with CsOH). The DVF bath solution used for
388 recording monovalent CatSper currents contained (in mM): 140 Cs-methanesulfonate, 40 HEPES, and
389 1 EDTA (pH 7.4, adjusted with CsOH). Baseline (leak) currents were recorded in HS before switching
390 to DVF. To evaluate the effects of mSEMG1 and its fragments, proteins (5 or 10 μM; 400–500 μL) were
391 diluted in DVF and added in real-time during the recordings. The complete compositions of the HS, DVF,

392 and pipette solutions are listed in Tables S1, S2, and S3. All electrophysiology recordings were
393 conducted at Washington University in St. Louis, School of Medicine, St. Louis, MO, USA.
394
395 **Membrane Potential assays**
396 Changes in sperm Em were assessed using DiSC3(5) (Molecular Probes, cat. #D306), as
397 previously described (Ritagliati et al., 2018). A sperm suspension aliquot (~4.0 x 10^6 cells) was diluted
398 in TYH medium supplemented with 20 mM sodium bicarbonate and 0.5% (m/v) BSA, with or without
399 mSEMG1 and its fragments (10 μM). Capacitated and non-capacitated sperm in the absence of
400 mSEMG1 were used as experimental controls. After treatment with the proteins and 30 min of
401 capacitation, cells were stained with the Em-sensitive dye DiSC3(5) 1 μM (Molecular Probes) for 2 min.
402 Spermatozoa were transferred to a cuvette at 37°C with mild agitation, and fluorescence was monitored
403 using a Cary Eclipse fluorescence spectrophotometer (Agilent, CA) at excitation/emission wavelengths
404 of 620/670 nm. Recordings began when steady-state fluorescence was reached, and calibration was
405 performed at the end of each measurement by adding 1 μM valinomycin with sequential KCl additions
406 for internal calibration curves. Sperm Em was derived from initial fluorescence (measured in arbitrary
407 fluorescence units) by linear interpolation of theoretical Em values from the calibration curve against
408 arbitrary fluorescence units for each trace. This internal calibration for each determination compensated
409 for variables influencing absolute fluorescence values.
410
411 **Statistical Analysis**
412 Data are presented as mean ± SEM. Normality and homoscedasticity were assessed using the
413 Kolmogorov–Smirnov test and F-test, respectively. Statistical differences between two independent
414 groups were analyzed using an unpaired Student's t-test; for comparisons involving more than two
415 groups, one-way ANOVA followed by Dunnett's post hoc test was used. For electrophysiological
416 recordings, a paired Student's t-test was applied. Percentage data were arcsine square root transformed
417 before statistical analysis (Zar, 2010). A p-value < 0.05 was considered statistically significant.
418
419 **Acknowledgments**
420 We thank Luiz Oliveira, Paulo Mioni, and Flávia Colenci, Ph.D., Department of Biophysics and
421 Pharmacology, IBB/UNESP, for their technical assistance. We are also grateful to Michael O´Rand,
422 Ph.D., and Katherine Hamil, M.Sc., for their critical reading of the manuscript and valuable insights, and
423 Célio Fernandes, Ph.D., for his helpful discussions during the project.
424
425 **Competing Interests**
426 The authors declare no competing or financial interests.

Funding

This study was funded by São Paulo Research Foundation (FAPESP, grants 2021/04746-3 and 2021/06718-7 to E.J.R.S, 2020/04841-3 and 2022/10159-6 to N.A.P.M, 2023/00125-0 to A.C.F.T., and 2023/04496-2 to N.C.M.S.), Coordenação de Aperfeiçoamento de Pessoal de Nível Superior (CAPES, grants 88887.496465/2020-00 and 88887.657625/2021-00 to A.D.A., J.J.A., and N.A.P.M.), Conselho Nacional de Desenvolvimento Científico e Tecnológico (CNPq, grants 303616/2022-9 and 442218/2023-0 to E.J.R.S and CNPq fellowship 201112/2024-8 to N.A.P.M.), Fondo para la Investigación Científica y Tecnológica (FICT, grant 2021-1-0102 to D.K.), and Barnes Jewish Hospital Foundation St. Louis (BJC, grant to P.V.L).

Data and resource availability

All relevant data and details of resources can be found within the article and its supplementary information. Any material (e.g., plasmids and recombinant proteins) generated in this paper can be obtained by emailing the corresponding author.

References

Araki, N., Trencsényi, G., Krasznai, Z. T., Nizsalóczki, E., Sakamoto, A., Kawano, N., Miyado, K., Yoshida, K. and Yoshida, M. (2015). Seminal Vesicle Secretion 2 acts as a protectant of sperm sterols and prevents ectopic sperm capacitation in mice. *Biol. Reprod.* **92**(1), 8, 1-10-18, 11-10. doi:10.1095/biolreprod.114.120642

Austin, C. R. (1952). The `Capacitation' of the mammalian sperm. *Nature* **170**(4321), 326-326. doi:10.1038/170326a0

Avenarius, M. R., Hildebrand, M. S., Zhang, Y., Meyer, N. C., Smith, L. L., Kahrizi, K., Najmabadi, H. and Smith, R. J. (2009). Human male infertility caused by mutations in the CATSPER1 channel protein. *Am. J. Hum. Genet.* **84**(4), 505-510. doi:10.1016/j.ajhg.2009.03.004

Bystroff, C. (2018). Intramembranal disulfide cross-linking elucidates the super-quaternary structure of mammalian CatSpers. *Reprod. Biol.* **18**(1), 76-82. doi:10.1016/j.repbio.2018.01.005

Cancel, A. M., Lobdell, D., Mendola, P. and Perreault, S. D. (2000). Objective evaluation of hyperactivated motility in rat spermatozoa using computer-assisted sperm analysis. *Human. Reprod.* **15**(6), 1322-1328. doi:10.1093/humrep/15.6.1322

Carlson, A. E., Quill, T. A., Westenbroek, R. E., Schuh, S. M., Hille, B. and Babcock, D. F. (2005). Identical phenotypes of CatSper1 and CatSper2 null sperm. *J. Biol. Chem.* **280**(37), 32238-32244. doi:10.1074/jbc.M501430200

Chang, M. C. (1951). Fertilizing capacity of spermatozoa deposited into the fallopian tubes. *Nature* **168**, 697. doi:10.1038/168697b0

Chávez, J. C., Ferreira, J. J., Butler, A., De La Vega Beltrán, J. L., Treviño, C. L., Darszon, A., Salkoff, L. and Santi, C. M. (2014). SLO3 K^+ channels control calcium entry through CATSPER channels in sperm. *J. Biol. Chem.* **289**(46), 32266-32275. doi:10.1074/jbc.M114.607556

Chung, J.-J., Miki, K., Kim, D., Shim, S.-H., Shi, H. F., Hwang, J. Y., Cai, X., Iseri, Y., Zhuang, X. and Clapham, D. E. (2017). CatSperζ regulates the structural continuity of sperm Ca^{2+} signaling domains and is required for normal fertility. *eLife* **6**, e23082. doi:10.7554/eLife.23082

Darszon, A., Nishigaki, T., Beltran, C. and Treviño, C. L. (2011). Calcium channels in the development, maturation, and function of spermatozoa. *Physiol. Rev.* **91**(4), 1305-1355. doi:10.1152/physrev.00028.2010

De Jonge, C. (2017). Biological basis for human capacitation-revisited. *Human Reprod. Update* **23**(3), 289-299. doi:10.1093/humupd/dmw048

de Lamirande, E. (2007). Semenogelin, the main protein of the human semen coagulum, regulates sperm function. *Semin Thromb Hemost* **33**(1), 60-68. doi:10.1055/s-2006-958463

de Lamirande, E. and Lamothe, G. (2010). Levels of semenogelin in human spermatozoa decrease during capacitation: involvement of reactive oxygen species and zinc. *Human. Reprod.* **25**(7), 1619-1630. doi:10.1093/humrep/deq110

Ferreira, Z., Seixas, S., Andrés, A. M., Kretzschmar, W. W., Mullikin, J. C., Cherukuri, P. F., Cruz, P., Swanson, W. J., Program, N. C. S., Clark, A. G., Green, E. D. and Hurle, B. (2013). Reproduction and Immunity-Driven Natural Selection in the Human WFDC Locus. *Molecular Biology and Evolution* **30**(4), 938-950. doi:10.1093/molbev/mss329

Freitas, M. J., Vijayaraghavan, S. and Fardilha, M. (2017). Signaling mechanisms in mammalian sperm motility. *Biol. Reprod.* **96**(1), 2-12. doi:10.1095/biolreprod.116.144337

Hildebrand, M. S., Avenarius, M. R., Fellous, M., Zhang, Y., Meyer, N. C., Auer, J., Serres, C., Kahrizi, K., Najmabadi, H., Beckmann, J. S. and Smith, R. J. (2010). Genetic male infertility and mutation of CATSPER ion channels. *Eur. J. Hum. Genet.* **18**(11), 1178-1184. doi:10.1038/ejhg.2010.108

Hwang, J. Y., Mannowetz, N., Zhang, Y., Everley, R. A., Gygi, S. P., Bewersdorf, J., Lishko, P. V. and Chung, J.-J. (2019). Dual sensing of physiologic pH and calcium by EFCAB9 regulates sperm motility. *Cell* **177**(6), 1480-1494.e1419. doi:10.1016/j.cell.2019.03.047

Katz, D. F. and Yanagimachi, R. (1980). Movement characteristics of hamster spermatozoa within the oviduct. *Biol. Reprod.* **22**(4), 759-764. doi:10.1095/biolreprod22.4.759

Kawano, N., Araki, N., Yoshida, K., Hibino, T., Ohnami, N., Makino, M., Kanai, S., Hasuwa, H., Yoshida, M., Miyado, K. and Umezawa, A. (2014). Seminal vesicle protein SVS2 is required for sperm survival in the uterus. *Proc. Natl. Acad. Sci. USA* **111**(11), 4145-4150. doi:10.1073/pnas.1320715111

Kawano, N., Yoshida, K., Iwamoto, T. and Yoshida, M. (2008). Ganglioside GM1 mediates decapacitation effects of SVS2 on murine spermatozoa. *Biol. Reprod.* **79**(6), 1153-1159. doi:10.1095/biolreprod.108.069054

Kawano, N. and Yoshida, M. (2007). Semen-coagulating protein, SVS2, in mouse seminal plasma controls sperm fertility. *Biol. Reprod.* **76**(3), 353-361. doi:10.1095/biolreprod.106.056887

Kent, K., Nozawa, K., Parkes, R., Dean, L., Daniel, F., Leng, M., Jain, A., Malovannaya, A., Matzuk, M. M. and T, X. G. (2024). Large-scale CRISPR/Cas9 deletions within the WFDC gene cluster uncover gene functionality and critical roles in mammalian reproduction. *Proc. Natl. Acad. Sci. USA* **121**(51), e2413195121. doi:10.1073/pnas.2413195121

Kirichok, Y. and Lishko, P. V. (2011). Rediscovering sperm ion channels with the patch-clamp technique. *Mol. Hum. Reprod.* **17**(8), 478-499. doi:10.1093/molehr/gar044

Kirichok, Y., Navarro, B. and Clapham, D. E. (2006). Whole-cell patch-clamp measurements of spermatozoa reveal an alkaline-activated Ca^{2+} channel. *Nature* **439**(7077), 737-740. doi:10.1038/nature04417

Lin, S., Ke, M., Zhang, Y., Yan, Z. and Wu, J. (2021). Structure of a mammalian sperm cation channel complex. *Nature* **595**(7869), 746-750. doi:10.1038/s41586-021-03742-6

Lishko, P. V. and Mannowetz, N. (2018). CatSper: a unique calcium channel of the sperm flagellum. *Curr. Opin. Physiol.* **2**, 109-113. doi:10.1016/j.cophys.2018.02.004

Liu, B., Mundt, N., Miller, M., Clapham, D. E., Kirichok, Y. and Lishko, P. V. (2021). Recording electrical currents across the plasma membrane of mammalian sperm cells. *J. Vis. Exp.* **168**. doi:10.3791/62049

López-González, I., Torres-Rodríguez, P., Sánchez-Carranza, O., Solís-López, A., Santi, C. M., Darszon, A. and Treviño, C. L. (2014). Membrane hyperpolarization during human sperm capacitation. *Mol. Hum. Reprod.* **20**(7), 619-629. doi:10.1093/molehr/gau029

Mannowetz, N., Naidoo, N. M., Choo, S.-A. S., Smith, J. F. and Lishko, P. V. (2013). Slo1 is the principal potassium channel of human spermatozoa. *eLife* **2**, e01009. doi:10.7554/eLife.01009

Mariani, N. A. P., Camara, A. C., Silva, A. A. S., Raimundo, T. R. F., Andrade, J. J., Andrade, A. D., Rossini, B. C., Marino, C. L., Kushima, H., Santos, L. D. and Silva, E. J. R. (2020). Epididymal protease inhibitor (EPPIN) is a protein hub for seminal vesicle-secreted protein SVS2 binding in mouse spermatozoa. *Mol. Cell. Endocrinol.* **506**, 110754. doi:10.1016/j.mce.2020.110754

Mitra, A., Richardson, R. T. and O'Rand, M. G. (2010). Analysis of recombinant human Semenogelin as an inhibitor of human sperm motility. *Biol. Reprod.* **82**(3), 489-496. doi:10.1095/biolreprod.109.081331

Navarro, B., Kirichok, Y. and Clapham, D. E. (2007). KSper, a pH-sensitive K^+ current that controls sperm membrane potential. *Proc. Natl. Acad. Sci. USA* **104**(18), 7688-7692. doi:10.1073/pnas.0702018104

Novero, A. G., Torres Rodríguez, P., De la Vega Beltrán, J. L., Schiavi-Ehrenhaus, L. J., Luque, G. M., Carruba, M., Stival, C., Gentile, I., Ritagliati, C., Santi, C. M., Nishigaki, T., Krapf, D., Buffone, M. G., Darszon, A., Treviño, C. L. and Krapf, D. (2024). The sodium–proton exchangers sNHE and NHE1 control plasma membrane hyperpolarization in mouse sperm. *J. Biol. Chem.* **300**(12), 107932. doi:10.1016/j.jbc.2024.107932

O'Rand, M. G. and Widgren, E. E. (2012). Loss of calcium in human spermatozoa via EPPIN, the semenogelin receptor. *Biol. Reprod.* **86**(2), 55, 51-57. doi:10.1095/biolreprod.111.094227

O'Rand, M. G., Widgren, E. E., Hamil, K. G., Silva, E. J. and Richardson, R. T. (2011). Epididymal protein targets: A brief history of the development of epididymal protease inhibitor as a contraceptive. *J. Androl.* **32**(6), 698-704. doi:10.2164/jandrol.110.012781

Quill, T. A., Sugden, S. A., Rossi, K. L., Doolittle, L. K., Hammer, R. E. and Garbers, D. L. (2003). Hyperactivated sperm motility driven by CatSper2 is required for fertilization. *Proc. Natl. Acad. Sci. USA* **100**(25), 14869-14874. doi:10.1073/pnas.2136654100

Ren, D., Navarro, B., Perez, G., Jackson, A. C., Hsu, S., Shi, Q., Tilly, J. L. and Clapham, D. E. (2001). A sperm ion channel required for sperm motility and male fertility. *Nature* **413**(6856), 603-609.

Ritagliati, C., Baro Graf, C., Stival, C. and Krapf, D. (2018). Regulation mechanisms and implications of sperm membrane hyperpolarization. *Mech. Dev.* **154**, 33-43. doi:10.1016/j.mod.2018.04.004

Robert, M. and Gagnon, C. (1999). Semenogelin I: a coagulum forming, multifunctional seminal vesicle protein. *Cell. Mol. Life Sci.* **55**(6), 944-960.

Sakaguchi, D., Miyado, K., Iwamoto, T., Okada, H., Yoshida, K., Kang, W., Suzuki, M., Yoshida, M. and Kawano, N. (2020). Human Semenogelin 1 promotes sperm survival in the mouse female reproductive tract. *Int. J. Mol. Sci.* **21**(11). doi:10.3390/ijms21113961

Silva, A. A. S., Raimundo, T. R. F., Mariani, N. A. P., Kushima, H., Avellar, M. C. W., Buffone, M. G., Paula-Lopes, F. F., Moura, M. T. and Silva, E. J. R. (2021). Dissecting EPPIN protease inhibitor domains in sperm motility and fertilizing ability: repercussions for male contraceptive development. *Mol. Hum. Reprod.* **27**(12), 1-15. doi:10.1093/molehr/gaab066

Silva, E. J. R., Hamil, K. G. and O'Rand, M. G. (2013). Interacting proteins on human spermatozoa: Adaptive evolution of the binding of semenogelin I to EPPIN. *PLoS One* **8**(12), e82014. doi:10.1371/journal.pone.0082014

Silva, E. J. R., Hamil, K. G., Richardson, R. T. and O'Rand, M. G. (2012). Characterization of EPPIN's Semenogelin I binding site: A contraceptive drug target. *Biol. Reprod.* **87**(3), 56, 51-58. doi:10.1095/biolreprod.112.101832

Stival, C., Puga Molina, L. d. C., Paudel, B., Buffone, M. G., Visconti, P. E. and Krapf, D. (2016). Sperm capacitation and acrosome reaction in mammalian sperm. *Sperm Acrosome Biogenesis and Function During Fertilization* (ed. Buffone, M. G.), pp. 93-106. Switzerland: Springer Cham.

Suárez, S. S. and Osman, R. A. (1987). Initiation of hyperactivated flagellar bending in mouse sperm within the female reproductive tract. *Biol. Reprod.* **36**(5), 1191-1198. doi:10.1095/biolreprod36.5.1191

Vickram, S., Rohini, K., Anbarasu, K., Dey, N., Jeyanthi, P., Thanigaivel, S., Issac, P. K. and Arockiaraj, J. (2022). Semenogelin, a coagulum macromolecule monitoring factor involved in the first step of fertilization: A prospective review. *Int. J. Biol. Macromol.* **209**, 951-962. doi:10.1016/j.ijbiomac.2022.04.079

Vyklicka, L. and Lishko, P. V. (2020). Dissecting the signaling pathways involved in the function of sperm flagellum. *Curr. Opin. Cell Biol.* **63**, 154-161. doi:10.1016/j.ceb.2020.01.015

Wang, D., Hu, J., Bobulescu, I. A., Quill, T. A., McLeroy, P., Moe, O. W. and Garbers, D. L. (2007). A sperm-specific Na^+/H^+ exchanger (sNHE) is critical for expression and *in vivo* bicarbonate regulation of the soluble adenylyl cyclase (sAC). *Proc. Natl. Acad. Sci. USA* **104**(22), 9325-9330. doi:10.1073/pnas.0611296104

Wang, H., McGoldrick, L. L. and Chung, J.-J. (2021). Sperm ion channels and transporters in male fertility and infertility. *Nat. Rev. Urol.* **18**(1), 46-66. doi:10.1038/s41585-020-00390-9

Wang, Z., Widgren, E. E., Sivashanmugam, P., O'Rand, M. G. and Richardson, R. T. (2005). Association of Eppin with Semenogelin on human spermatozoa. *Biol. Reprod.* **72**(5), 1064-1070. doi:10.1095/biolreprod.104.036483

584 **Young, S., Schiffer, C., Wagner, A., Patz, J., Potapenko, A., Herrmann, L., Nordhoff, V., Pock, T.,**
585 **Krallmann, C., Stallmeyer, B., Röpke, A., Kierzek, M., Biagioni, C., Wang, T., Haalck, L., Deuster,**
586 **D., Hansen, J. N., Wachten, D., Risse, B., Behre, H. M., Schlatt, S., Kliesch, S., Tüttelmann, F.,**
587 **Brenker, C. and Strünker, T.** (2024). Human fertilization in vivo and in vitro requires the CatSper
588 channel to initiate sperm hyperactivation. *J. Clin. Invest.* **134**(1). doi:10.1172/JCI173564

589 **Zar, J. H.** (2010). *Biostatistical Analysis*. New Jersey, USA: Pearson Prentice Hall.

590 **Zhao, Y., Wang, H., Wiesehoefer, C., Shah, N. B., Reetz, E., Hwang, J. Y., Huang, X., Wang, T.-e.,**
591 **Lishko, P. V., Davies, K. M., Wennemuth, G., Nicastro, D. and Chung, J.-J.** (2022). 3D structure and
592 in situ arrangements of CatSper channel in the sperm flagellum. *Nat. Commun.* **13**(1), 3439.
593 doi:10.1038/s41467-022-31050-8

594

595 **Figure Legends**

596 **Figure 1. Effects of mSEMG1 on murine sperm motility and viability.** (A and B) Percentage of total
597 and slow motility of spermatozoa after incubation with mSEMG1. (C) Percentage of viable spermatozoa
598 after incubation with mSEMG1. Spermatozoa were incubated in capacitating HTF medium in the
599 absence (control) or presence of increasing concentrations of mSEMG1 (1, 3, 10, and 25 μM). Sperm
600 motility was assessed after 20 and 120 min of capacitation, while sperm viability was assessed after
601 120 min. Dots with the same color represent the values from an independent experiment. Asterisks
602 indicate statistically significant differences from the control group ($p<0.05$, ANOVA followed by Dunnett´s
603 test). Percentage data were transformed using arcsine square-root values before statistical analysis.
604 Results are presented as mean ± SEM values from independent experiments using sperm samples from
605 3-7 mice.

606

607 **Figure 2. Effects of mSEMG1 on hyperactivated motility.** (A) Percentage of hyperactivated motility
608 of spermatozoa after incubation with mSEMG1. (B) Concentration-response curve of hyperactivated
609 motility rate of spermatozoa after incubation with mSEMG1. Data were expressed as mean percentage
610 values relative to the control group. Inhibitory concentration 50% (IC_{50}, 95% confidence interval) is
611 presented. (C) Curvilinear velocity (VCL) (left) and amplitude of lateral head displacement (ALH) (right)
612 of spermatozoa after incubation with mSEMG1. Spermatozoa were isolated from the cauda epididymidis
613 and incubated in capacitating HTF medium in the absence (control) or presence of increasing
614 concentrations of mSEMG1 (1, 3, 10, and 25 μM). (D) Percentage of hyperactivated spermatozoa in the
615 presence or absence of NH_4Cl. Cells were incubated in non-capacitating medium (Non-Cap),
616 supplemented or not with NH_4Cl (left), or in capacitating medium (Cap), supplemented or not with NH_4Cl
617 in the absence or presence of 10 μM mSEMG1 (right). Sperm motility was assessed after 30 and 120
618 min of capacitation. Dots with the same color represent the values from an independent experiment.
619 Asterisks indicate statistically significant differences from the control group ($p<0.05$, ANOVA followed
620 by Dunnett´s test). Percentage data were transformed using arcsine square-root values before statistical
621 analysis. Results are presented as mean ± SEM values from independent experiments using sperm
622 samples from 3-6 mice.

623

624 **Figure 3. Effects of mSEMG1 on $I_{CatSper}$.** (A) Representative DIC image of murine spermatozoon with
625 cytoplasmic droplet (yellow circle) used for patch-clamp recording. Right: Cs^+ concentration and pH of
626 the pipette and bath solutions are indicated. Voltage ramps (-80 mV to 80 mV, 1 s) were applied in HS
627 and in DVF to record $I_{CatSper}$. Baseline currents were recorded in HS (black), which lacked $I_{CatSper}$ due to
628 its inhibition by extracellular magnesium. (B) Left: $I_{CatSper}$ recordings in response to voltage ramps in DVF
629 before (control) (red) and after addition of 5 μM mSEMG1 (blue), including washout (grey), and recorded

630 from wild-type and CatSper KO (inset) spermatozoa. Traces represent recordings from the same
631 spermatozoon. Right: $I_{CatSper}$ recordings (mean ± SEM; pA) obtained at −80 mV in DVF solution before
632 and after exposure to 5 μM mSEMG1. $I_{CatSper}$ recording was repeated in DVF after mSEMG1 was
633 washed out. Sperm cell capacitance ranged from 2.0 to 2.6 pF. Dots with the same color represent
634 current values from the same cell. (C) Current-voltage (I-V) relationships were calculated from
635 amplitudes shown in panel A in the DVF solution before and after 5 μM mSEMG1 treatment. (D)
636 Quantification of membrane potential (Em) in non-capacitated, capacitated, and capacitated
637 spermatozoa treated with 10 μM mSEMG1. Membrane potential was assessed after 30 min of
638 capacitation. Dots with the same color represent values from independent experiments. Asterisks
639 indicate statistically significant differences from the control group ($p < 0.05$, ANOVA followed by
640 Dunnett's test or paired t-test). Results are presented as mean ± SEM from independent experiments
641 using sperm samples from 3-4 mice.
642
643 **Figure 4. Mouse SEMG1 sequence, recombinant constructs, and their effects on sperm motility.**
644 (A) Left: Amino acid sequence of mouse SEMG1. The signal peptide is shown in lowercase letters.
645 Amino acid repeats are indicated in bold. The GGS region is underlined, while the KS region and the
646 single cysteine residue are highlighted in red and yellow, respectively. Right: Schematic representation
647 of mSEMG1 full-length and truncated constructs used in the experiments. The mSEMG1 constructs
648 include a 6x-His tag. (B) Percentage of total motile (left) and hyperactivated (right) spermatozoa after
649 incubation with mSEMG1. (C) Curvilinear velocity (VCL) (left) and amplitude of lateral head
650 displacement (ALH) (right) of spermatozoa after incubation with mSEMG1 constructs. Spermatozoa
651 were isolated from the cauda epididymidis and incubated in capacitating HTF medium in the absence
652 (control) or presence of mSEMG1 constructs (25 μM). Sperm motility was assessed after 120 min. Dots
653 with the same color represent the values from an independent experiment. Asterisks indicate statistically
654 significant differences from the control group ($p<0.05$, ANOVA followed by Dunnett´s test). Percentage
655 data were transformed using arcsine square-root values before statistical analysis. Results are
656 presented as mean ± SEM values from independent experiments using sperm samples from 3-5 mice.
657
658 **Figure 5. Effects of mSEMG1 fragments on $I_{CatSper}$.** (A-C) Left: Representative $I_{CatSper}$ recordings in
659 response to voltage ramps in DVF (control) before (red) and after 5 μM $mSEMG1^{Q32–V118}$ (pink),
660 $mSEMG1^{R98–G375}$ (green), and $mSEMG1^{Y221–G375}$ (orange), recorded from wild-type mouse spermatozoa.
661 Baseline currents are recorded in HS (black). Traces represent recordings from the same
662 spermatozoon. Right: Quantification of $I_{CatSper}$ (mean ± SEM; pA) at −80 mV in DVF solution before and
663 after addition of the respective mSEMG1 fragments. Sperm cell capacitance ranged from 2.1 to 2.8 pF.
664 Dots with the same color represent values from independent experiments. Asterisks indicate statistically

665 significant differences from the control group ($p < 0.05$, paired t-test). Results are presented as mean ±
666 SEM from independent experiments using sperm samples from 4-7 mice.
667
668 **Figure 6. Characterization of the interaction between mSEMG1 and mEPPIN.** (A) Schematic
669 representation of the AlphaScreen assay. GST-tagged mEPPIN was captured by anti-GST acceptor
670 beads, and 6×His-tagged mSEMG1 by Ni^{2+}-chelate donor beads. Upon excitation at 680 nm, a
671 luminescent signal was generated due to the proximity (<200 nm) of donor and acceptor beads,
672 indicating an interaction between mEPPIN and mSEMG1. (B) mEPPIN was incubated with mSEMG1 in
673 a time-course experiment. Background signal was detected when beads were incubated in the absence
674 of mEPPIN or mSEMG1. Data are presented as mean ± SEM from a representative experiment out of
675 ten, each performed in triplicate. (C) Left: Concentration-response curve for mSEMG1 with a constant
676 concentration of mEPPIN (10 nM). Right: Concentration-response curve for mEPPIN with a constant
677 concentration of mSEMG1 (30 nM). A specific signal for each data point was determined by subtracting
678 the background signal from the total signal. Results represent mean ± SEM of specific signals from 2-4
679 experiments. (D) Left: mSEMG1 and its fragments (Q32-V118: $mSEMG1^{Q32-V118}$, R98-G375:
680 $mSEMG1^{R98-G375}$, and Y221-G375: $SEMG^{Y221-G375}$) were incubated with mEPPIN for 4 h. Right: mEPPIN
681 and its N-terminal construct (L24-K68: $mEPPIN^{L24-K68}$) were incubated with mSEMG1 for 4 h. Dots with
682 the same color represent values from independent experiments. Specific signals for each data point
683 were normalized as a percentage of the signal from full-length mSEMG1/mEPPIN binding. Asterisks
684 indicate statistically significant differences from the control group (mSEMG1 or mEPPIN) ($p<0.05$,
685 ANOVA followed by Dunnett´s test). Results are expressed as mean ± SEM of specific signals from 4-
686 10 experiments. Cps = counts per second.
687
688 **Figure 7. Working model of SEMG1-mediated inhibition of sperm hyperactivation after sperm**
689 **ejaculation.** EPPIN is present on the surface of mature spermatozoa stored in the cauda epididymidis.
690 In the semen coagulum/copulatory plug (Phase 1), SEMG1 binds to the sperm surface via interaction
691 with EPPIN through a binding domain within residues R98-S220, thus coating spermatozoa. SEMG1
692 may also interact with spermatozoa independently of EPPIN binding. Domains within the SEMG1 Q32-
693 G375 and R98-S220 regions inhibit sperm function, i.e., temporarily preventing hyperactivation in the
694 uterus by inhibiting CatSper, while only the R98-S220 domain contains the EPPIN binding site. As
695 spermatozoa move to the upper regions of the female reproductive tract, SEMG1 is proteolytically
696 cleaved by a PSA-like enzyme (Phase 2), whose identity remains unknown in mice, allowing
697 hyperactivation to take place in the oviduct.

A

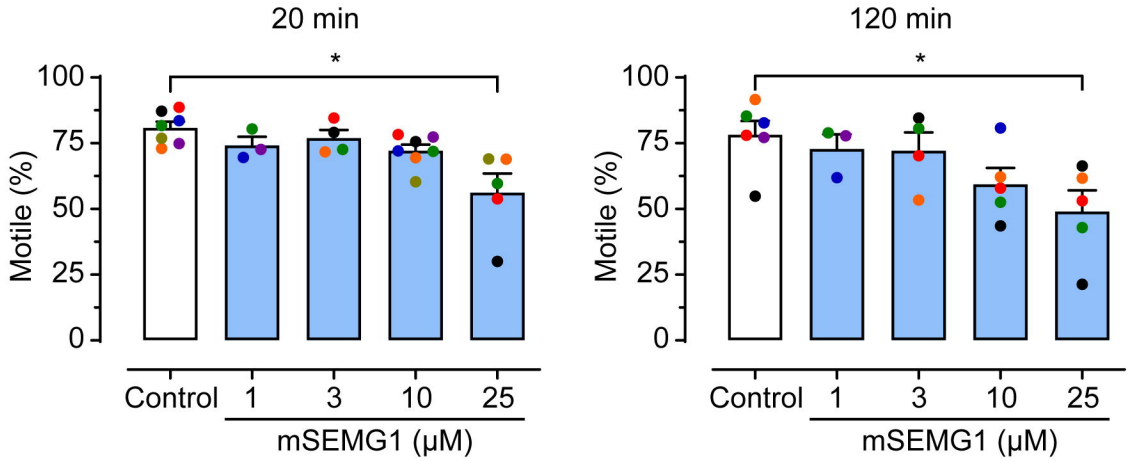
20 min
120 min
Motile (%)
100
75
50
25
0
*
Control
1
3
10
25
mSEMG1 (μM)

B

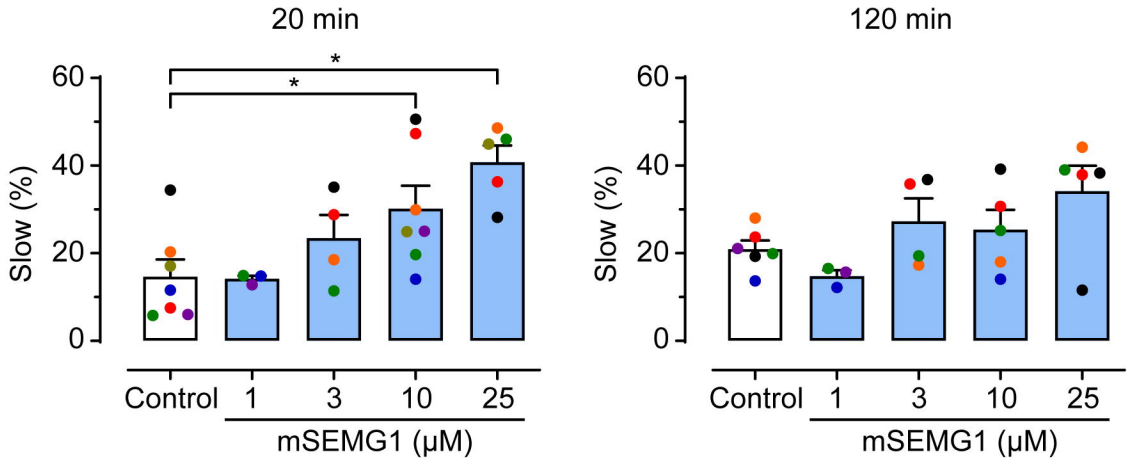
20 min
120 min
Slow (%)
60
40
20
0
*
*
Control
1
3
10
25
mSEMG1 (μM)

C

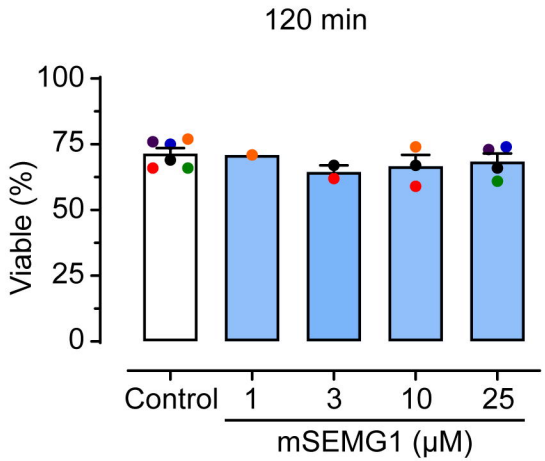
120 min
Viable (%)
100
75
50
25
0
Control
1
3
10
25
mSEMG1 (μM)

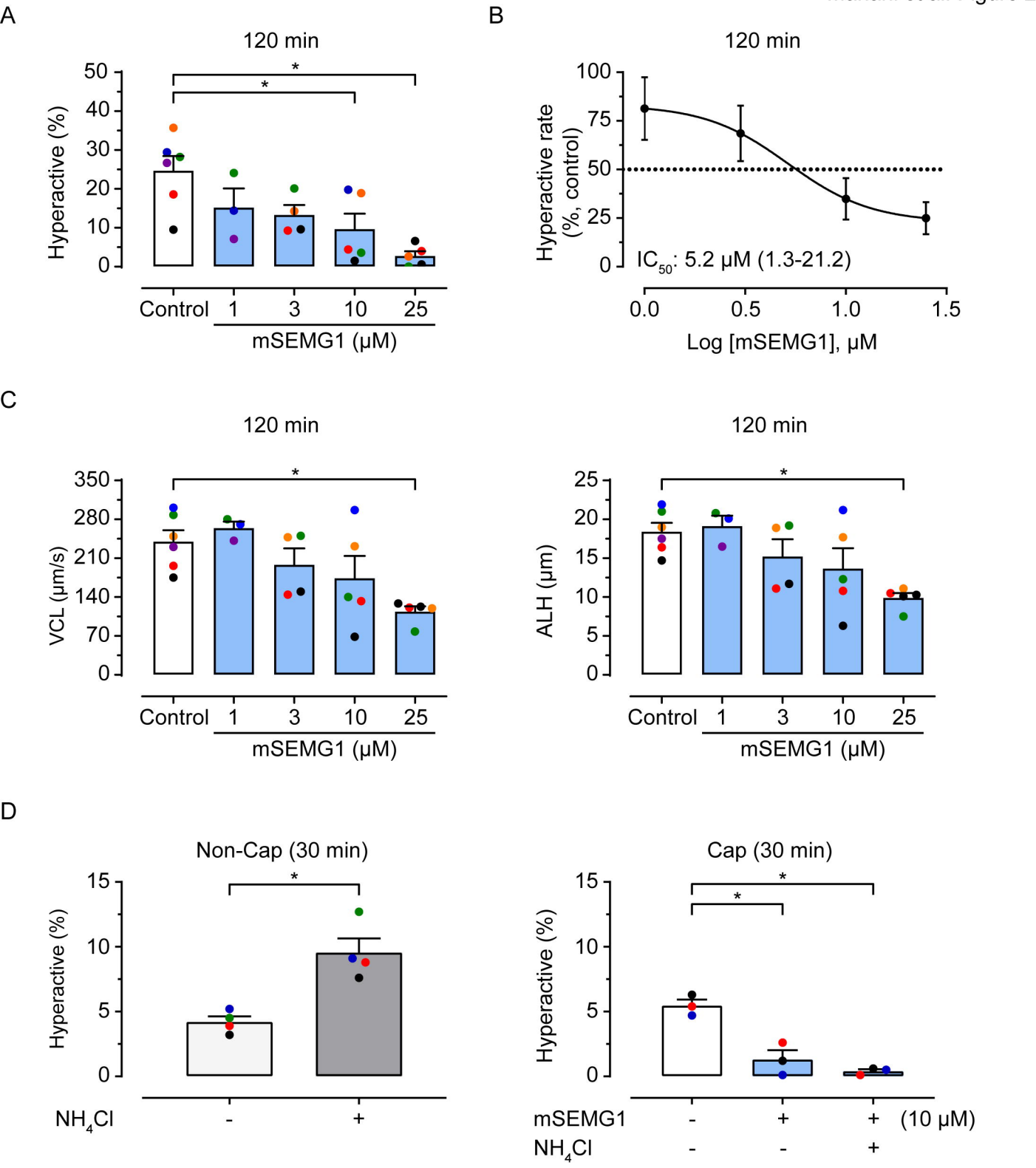
A
120 min
Hyperactive (%)
50
40
30
20
10
0
*
*
Control
1
3
10
25
mSEMG1 (μM)
B
120 min
Hyperactive rate (%, control)
100
75
50
25
0
IC50: 5.2 μM (1.3-21.2)
0.0
0.5
1.0
1.5
Log [mSEMG1], μM
C
120 min
VCL (μm/s)
350
280
210
140
70
0
*
Control
1
3
10
25
mSEMG1 (μM)
120 min
ALH (μm)
25
20
15
10
5
0
*
Control
1
3
10
25
mSEMG1 (μM)
D
Non-Cap (30 min)
Hyperactive (%)
15
10
5
0
*
NH4Cl
-
+
Cap (30 min)
Hyperactive (%)
15
10
5
0
*
*
mSEMG1
-
+
+
(10 μM)
NH4Cl
-
-
+

A

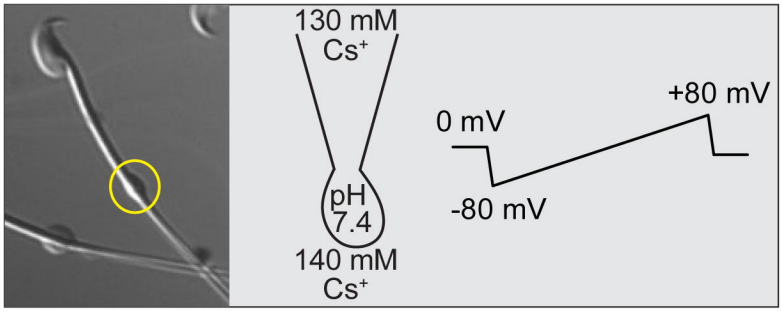
130 mM
Cs+
pH
7.4
140 mM
Cs+
0 mV
-80 mV
+80 mV

B

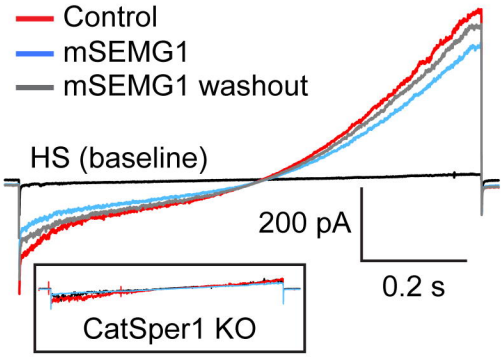
Control
mSEMG1
mSEMG1 washout
HS (baseline)
200 pA
0.2 s
CatSper1 KO

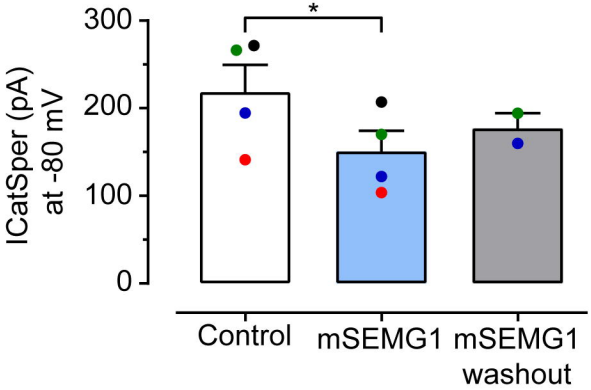
ICatSper (pA)
at -80 mV
300
200
100
0
*
Control
mSEMG1
mSEMG1
washout

C

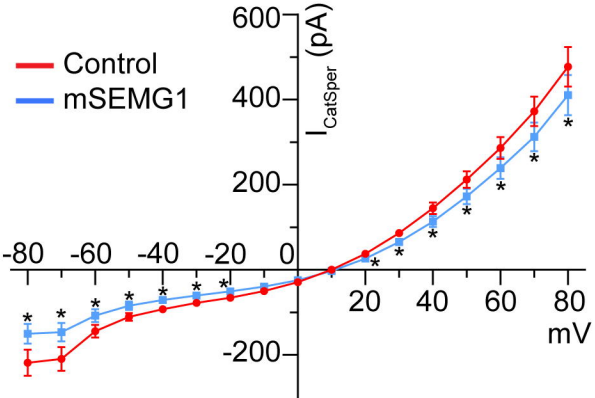
Control
mSEMG1
I CatSper (pA)
600
400
200
-200
-80
-60
-40
-20
0
20
40
60
80
mV

D

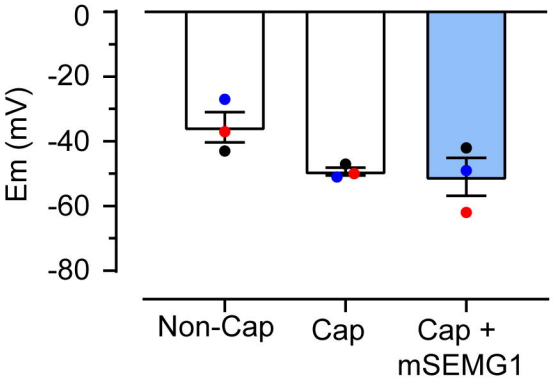
Em (mV)
0
-20
-40
-60
-80
Non-Cap
Cap
Cap +
mSEMG1

A

SEMG1 (*Mus musculus*, NP_059086)

```
1...................20...................40...................60
mkssvfvlslllilerqsavvgQYGATKGNFQSSSSEGFMLGQKGRLSFGIKGGSDEAAE
61..................80...................100..................120
ESLFMQSQRRVYGQGGGDMTQTRVSQEHTSVKGAAILCRNGQVSQLKSQESQIKSYGQVKS
121.................140..................160..................180
SGQLKSGGSAFGQVKSSVSQIKSYGQLKSGGQLKSGGPAFGQVKSQESQIKSYGQLKSSG
181.................200..................220..................240
QLKSGGSAFGQVKSSVSQIKSYGQLKSGGSQVKSYGQTKSYGEEGQLNSFSQLKSQGAQL
241.................260..................280..................300
KSYGQQKSQQQSSFSQVKSQSSQLKSYGQQKSLKGFSQQTQHKGFAMDEGMSQVRKQFSD
301.................320..................340..................360
DDLSVQQKSTQQMKTEEDLSQFGQQRQYGQERSQSYKGYLEQYRKKVQEQQRKNFNPGNY
361...........375
FTKGGADLYQAQLKG
```

Recombinant mouse SEMG1 constructs

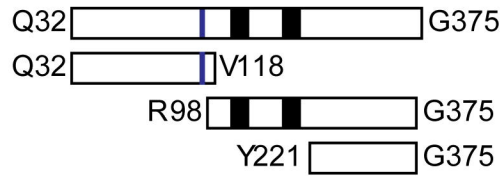

B

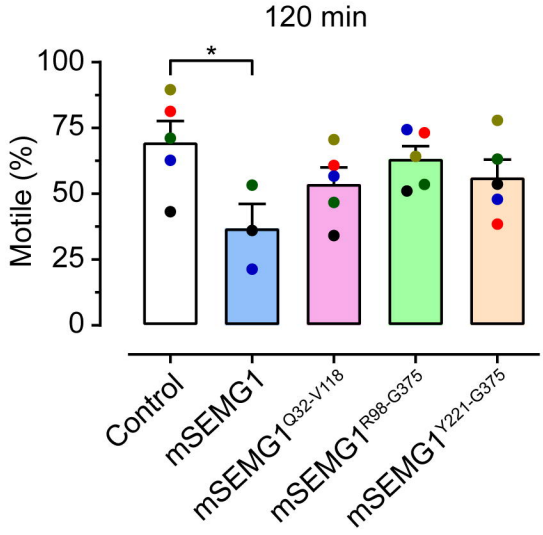

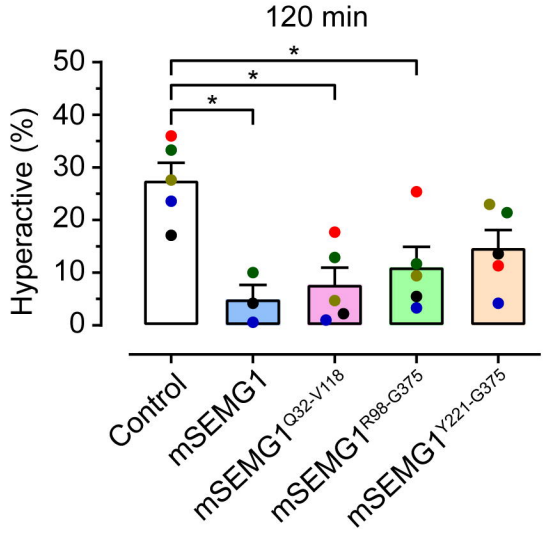

C

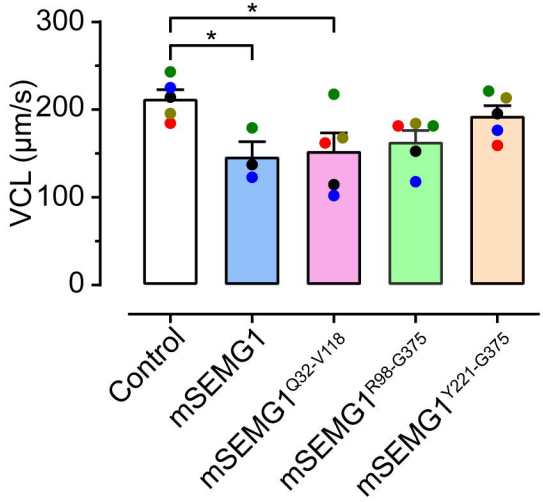

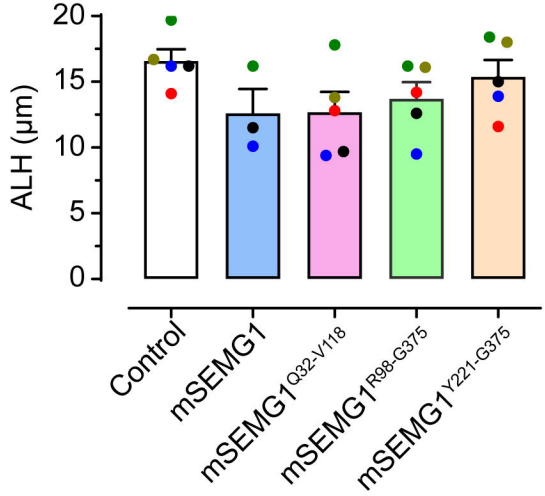

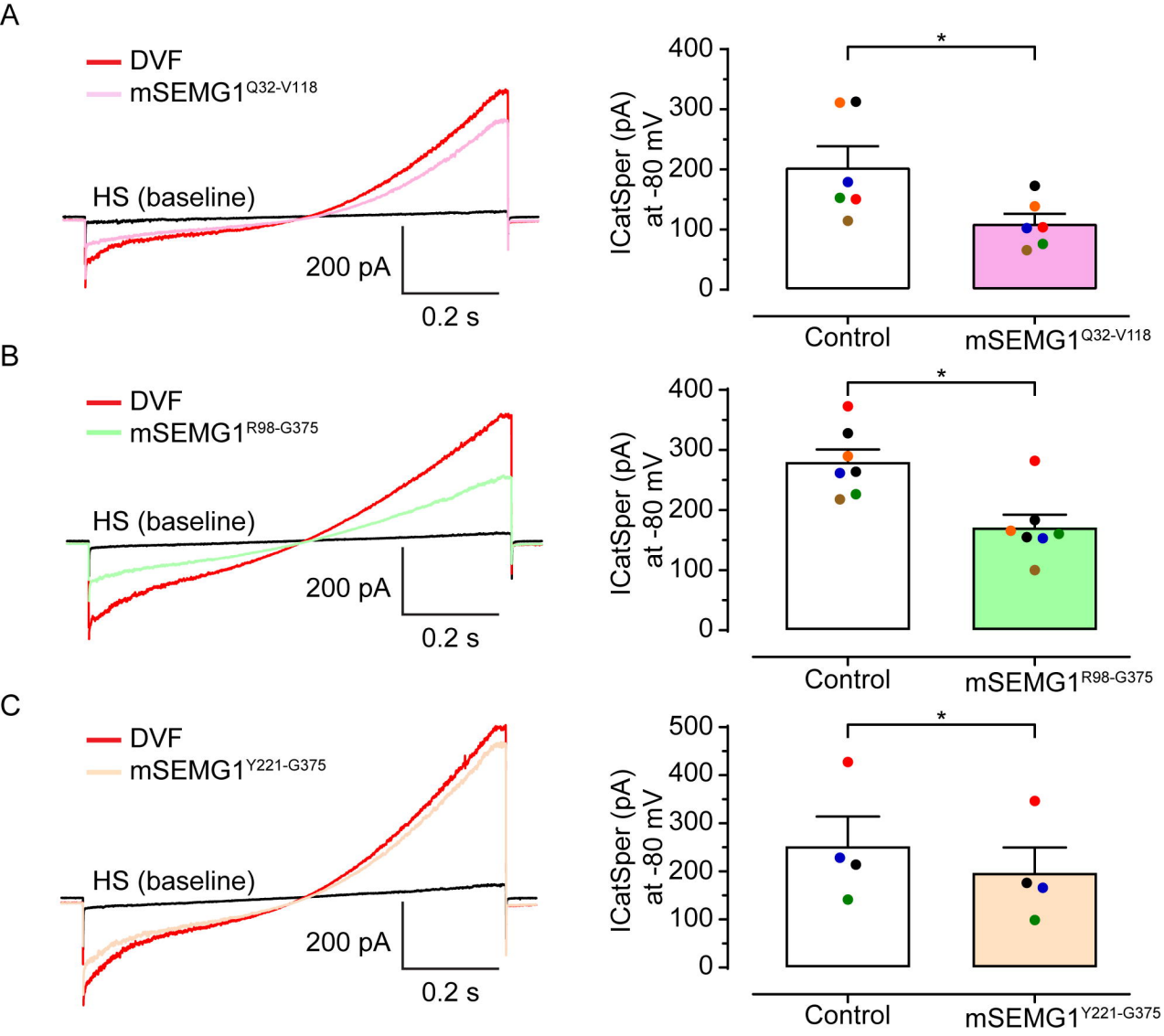
A
DVF
mSEMG1Q32-V118
HS (baseline)
200 pA
0.2 s
ICatSper (pA) at -80 mV
400
300
200
100
0
*
Control
mSEMG1Q32-V118
B
DVF
mSEMG1R98-G375
HS (baseline)
200 pA
0.2 s
ICatSper (pA) at -80 mV
400
300
200
100
0
*
Control
mSEMG1R98-G375
C
DVF
mSEMG1Y221-G375
HS (baseline)
200 pA
0.2 s
ICatSper (pA) at -80 mV
500
400
300
200
100
0
*
Control
mSEMG1Y221-G375

A

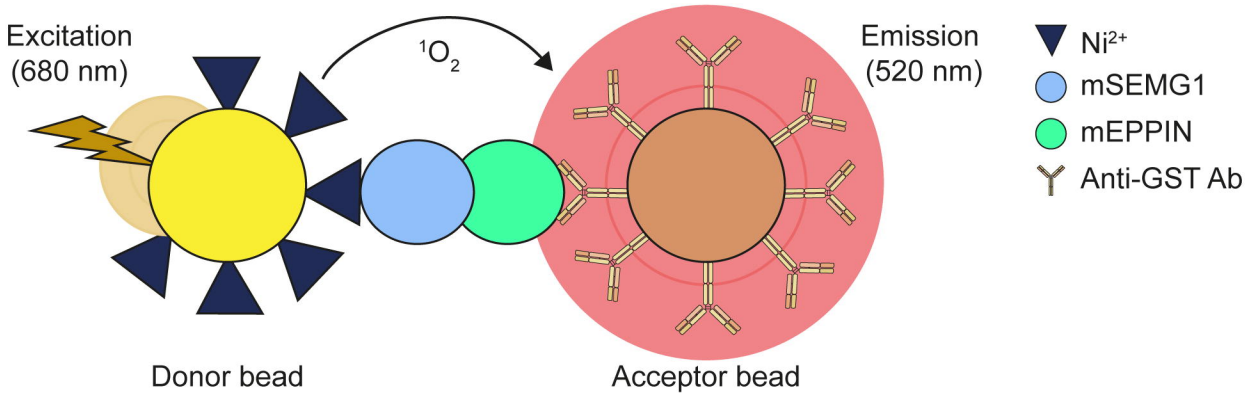
Excitation
(680 nm)
$^1O_2$
Emission
(520 nm)
Ni2+
mSEMG1
mEPPIN
Anti-GST Ab
Donor bead
Acceptor bead

B

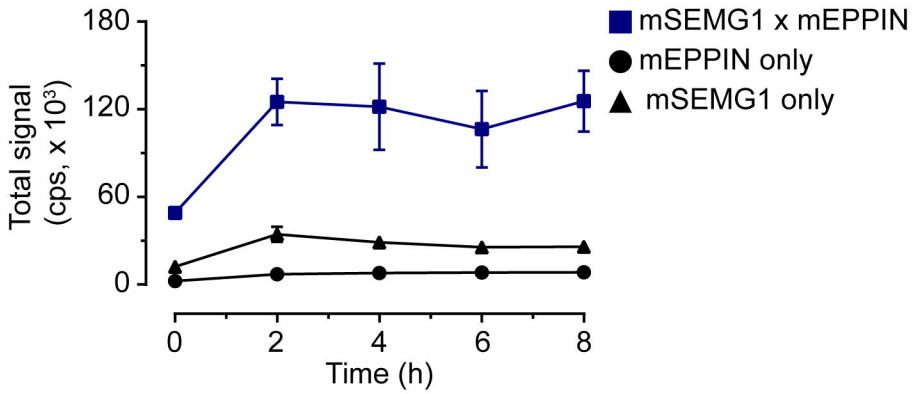
mSEMG1 x mEPPIN
mEPPIN only
mSEMG1 only
Total signal
(cps, x 10³)
180
120
60
0
0
2
4
6
8
Time (h)

C

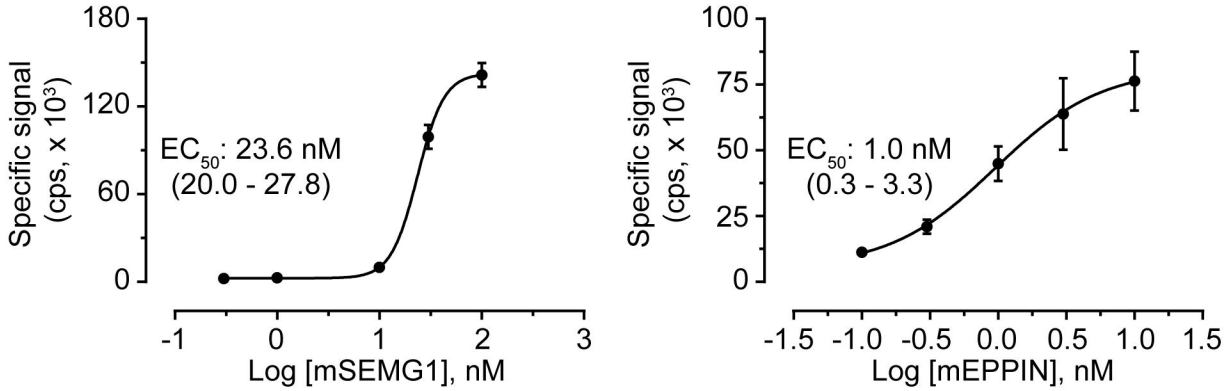
Specific signal
(cps, x 10³)
EC50: 23.6 nM
(20.0 - 27.8)
Log [mSEMG1], nM
EC50: 1.0 nM
(0.3 - 3.3)
Log [mEPPIN], nM

D

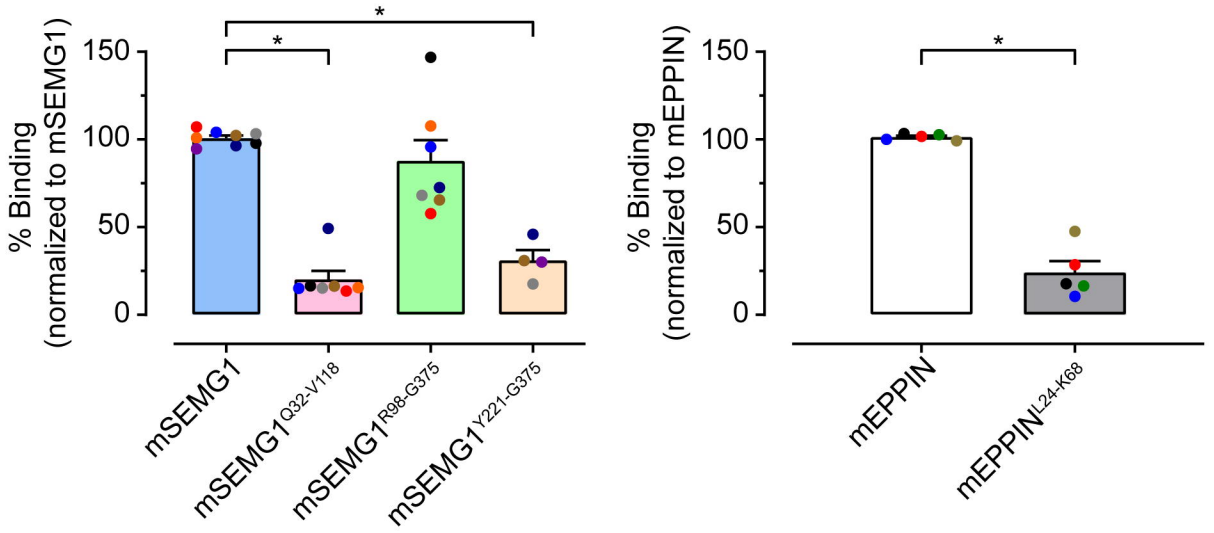
% Binding
(normalized to mSEMG1)
% Binding
(normalized to mEPPIN)
mSEMG1
mSEMG1Q32-V118
mSEMG1R98-G375
mSEMG1Y221-G375
mEPPIN
mEPPINL24-K68
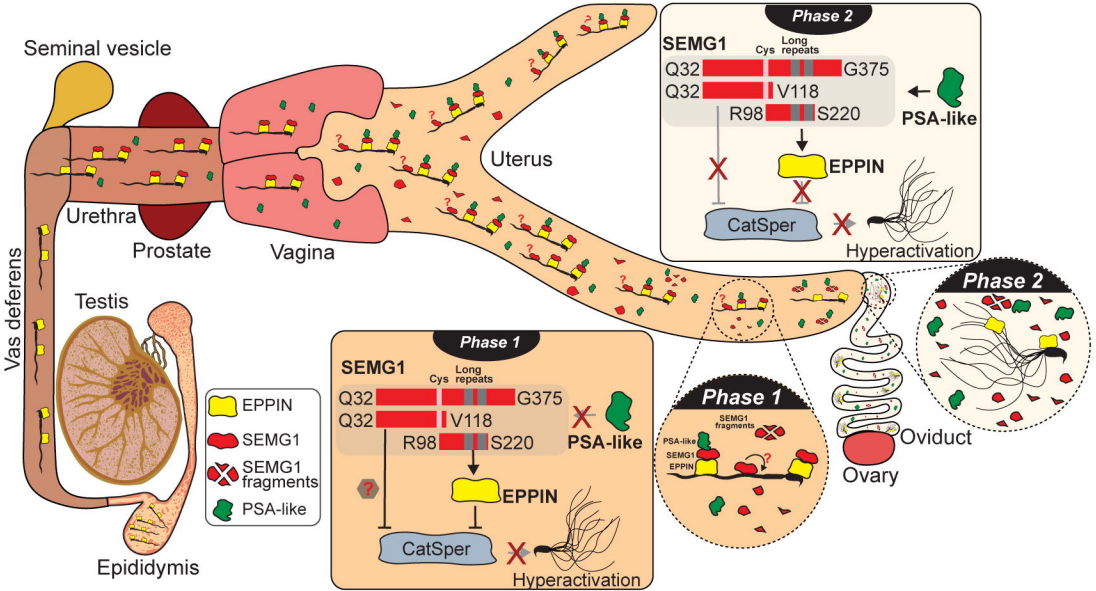
Mariani et al. Figure 7